

In Vitro Dissolution Kinetics of Captopril from Microspheres Manufactured by Solvent Evaporation

e-mail: R.B.Walker@ru.ac.za

Sandile M. Khamanga and Roderick B. Walker*

Faculty of Pharmacy, Rhodes University, P.O. Box 94, Grahamstown, South Africa, 6140

ABSTRACT

The aim of this study was to develop and assess captopril-loaded microspheres in which Methocel and Eudragit RS were used as release-controlling factors and to evaluate captopril (CPT) release using kinetic models. Drug-excipient interactions were evaluated using infrared studies, and the physical appearance was characterized using scanning electron microscopy (SEM). A burst effect was observed during the first stage of dissolution for most batches of microspheres. SEM results reveal that this may be attributed to dissolution of captopril crystals that were present on the surface, embedded in the superficial layer of the matrix materials, trapped near the surface of the microspheres, or that may have diffused rapidly through the porous surface of the capsules. The release data generated during in vitro release studies were fitted to zero-order, first-order, Higuchi, Korsmeyer–Peppas, Kopcha, and Makoid–Banakar models. The release kinetics of captopril from most formulations followed a classical Fickian diffusion mechanism. SEM photographs showed that diffusion took place through pores located in the surface of the microcapsules. The Kopcha model diffusion and erosion terms showed a predominance of diffusion relative to swelling or erosion throughout the entire test period. The drug release mechanism was also confirmed by the Makoid–Banakar and Korsmeyer–Peppas model exponents. This further supports a diffusion–release mechanism for most formulations. The models postulate that the total drug released is a summation of several mechanisms (viz., burst release, relaxation-induced controlled release, and diffusional release). These results also support the potential application of Eudragit/Methocel microspheres as a suitable sustained-release drug delivery system for captopril.

INTRODUCTION

Solid oral dosage forms remain the most convenient means of treatment available. The effectiveness of these dosage forms relies on dissolution of a drug in gastrointestinal tract fluids before absorption into the systemic circulation. The rate of dissolution of a drug from a solid dosage form is therefore crucial for optimization of therapy.

Over the past three decades, dissolution testing has evolved into a powerful tool for characterizing the quality of oral pharmaceutical products. The term dissolution can be defined as a process in which a known amount of drug dissolves in a given medium per unit time under standardized conditions (1).

In vitro dissolution is one of the most important elements of the drug development process. Several models may be used to describe dissolution profiles where $f(t)$ is a function of t (time) that is related to the amount of drug dissolved from a dosage form. The quantitative interpretation of values generated in dissolution studies is facilitated by the use of generic equations that translate dissolution curves mathematically as a function of certain parameters related to the dosage forms under investigation. In some cases, the equations can be deduced by a theoretical analysis of the processes to which a dosage form is subjected. A water-soluble drug incorporated into a hydrophilic matrix is released mainly by a diffusion-controlled process,

whereas for a poorly water-soluble compound, the principal mechanism of release is a function of erosion of the matrix that carries the drug (2).

Dissolution testing is now an established and standardized method for measuring drug product performance (3) and permits the comparison of results for different batches of the same product, similar products from different suppliers, or results from different laboratories. Dissolution testing is therefore a useful tool for quality control and in formulation development, and the FDA has made it a regulatory requirement in the approval of new drug products. However, as dissolution testing is an empirical method of evaluation, it has some drawbacks when used in formulation development. For example, existing empirical data or formulas may be of little help when evaluating each new formulation, and a novel series of tests may have to be developed and performed when assessing these products. For every dissolution test, the product to be tested must have already been manufactured. Both these aspects add significantly to the time and cost of bringing a new drug to market. In general, dissolution studies must be based on the specific conditions that are required to study a particular drug compound and include the selection of appropriate media, apparatus, and operating variables (4–7). In addition and where possible, dissolution studies should be performed following the specifications outlined in the *United States Pharmacopeia (USP)*.

Dissolution from a dosage form involves two steps, liberation of the drug from the formulation matrix

*Corresponding author.

(disintegration) followed by the dissolution of the drug (solubilization of the drug particles) in the liquid medium. The overall rate of dissolution depends on the slower of these two steps. The cohesive properties of the formulated drug play a key role in liberation, and for solid dosage forms, these include disintegration and erosion. If this step of dissolution is rate limiting, then the rate of dissolution is considered disintegration-controlled. Whereas if in the solubilization of drug particles, the physicochemical properties of a drug such as its chemical form (e.g., salt, free acid, free base), physical form (e.g., amorphous or polymorph and primary particle size), or both play an important role, then the rate of release is dissolution-limited (8).

Models that best describe drug-release phenomena must be used to define drug-release mechanisms (9) as this helps to analyze and explain mathematically the processes that occur when a drug is released from a dosage form. In this study, several mathematical models were used to elucidate the mechanism(s) of CPT release from the batches of microspheres that were manufactured.

To optimize the formulation and manufacture of CPT microspheres, a central composite design (CCD) approach was used in a multivariate experimental design to establish the number and formulas that were to be manufactured. In this study, the modeling of percent drug released and the optimization of drug released was undertaken using mathematical methods. Optimization of the formulations was performed by selecting formulations based on the criterion of attaining a maximum value for the percent drug released.

CPT is a competitive inhibitor of angiotensin-converting enzyme (ACE) (10, 11) and is routinely used for the management of hypertension and congestive heart failure. It is commercially available as immediate-release tablets in doses of 12.5–50 mg (12) and has a short elimination half-life following oral administration. Consequently, CPT may be a suitable candidate for inclusion in sustained-release dosage forms. The development of a once-daily CPT formulation for oral administration would be a significant advantage in the promotion of patient adherence. Furthermore, the added advantage of minimization of side effects and reduced fluctuations in blood levels on long-term therapy may well result in better therapeutic outcomes (13).

CPT is well absorbed from the proximal small intestines (14). It is known as 1-[3-mercapto-2-(S)-methyl-1-oxopropyl]-S-(L)-proline (14, 15) and is a white crystalline powder that has a slight sulfurous odor (14). CPT has an aqueous solubility of 160 mg/mL at 25 °C (16), and a plot of solubility versus temperature is linear up to 40 °C, above which CPT shows extraordinarily high water solubility (17). The chemical structure of CPT (18) is depicted in Figure 1.

The main objective of the present investigation was to evaluate the *in vitro* release characteristics of CPT-loaded microspheres manufactured using a solvent evaporation technique.

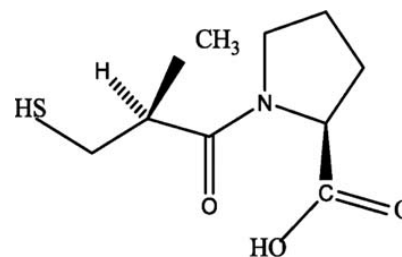


Figure 1. Chemical structure of captopril ($C_9H_{15}NO_3S$, $MW = 217.3$).

Materials

CPT powder was donated by Protea Chemicals (Midrand, South Africa). Hydroxypropyl methylcellulose (Methocel K100M and K15M) was donated by Colorcon Ltd (Dartford, Kent, UK). Microcrystalline cellulose (Avicel 101) was purchased from FMC (Philadelphia, USA). Eudragit RS was donated by Rohm Pharma (GmbH, Darmstadt, Germany). Span 80 was purchased from Sigma–Aldrich (GmbH, Germany). Liquid paraffin was supplied by ADC Laboratories (Durban, South Africa). Acetone AR was purchased from Associated Chemical Enterprises (Southdale, South Africa), *n*-hexane was acquired from Burdick and Jackson Laboratories (Michigan, USA), and dimethyl polysiloxane was purchased from Sigma–Aldrich (Kempton Park, South Africa). All chemicals were used without any further purification.

Methods

Infrared Spectroscopy (IR)

Prior to manufacture, IR was used to study the compatibility of CPT with excipients to be used for the manufacture of the microspheres. IR spectra were recorded using the KBr disc method over the wavelength range of 4000–400 cm^{-1} , and spectra were recorded using a Bruker Model Verter 70 instrument (Beaconsfield, Bucks, England). The microscopic spectrophotometer was equipped with a TENSOR 27 RT-Dlatgs detector. The velocity of the scanner was set at 10 kHz. Sample combinations showing promise in terms of compatibility were collected successively from the actual analysis area by mapping.

Manufacture of Microspheres

The manufacture of microspheres was achieved using an emulsification and solvent evaporation technique based on the method reported by Khamanga et al. (19). Design Expert software package (version 7.1, State–Ease Inc., Minneapolis, MN, USA) was used to generate the experiments, and the representative formulations used to manufacture the microspheres are listed in Table 1. To manufacture all 30 formulations, 0.75 g of CPT and 0.5 g of microcrystalline cellulose (MCC), as filler and binder, were included in the formulation. The amount of CPT and MCC were kept constant throughout the manufacturing process.

The different polymer proportions and the MCC were dispersed in 20 mL of acetone, and an accurately weighed

Table 1. Formulation Composition and Homogenizing Speed Used to Manufacture Microcapsules

RUN	Eudragit RS	Methocel K100M	Methocel K15M	Homogenizing Speed
	g	g	g	rpm (1000)
1	2.0	0.50	0.50	1.5
2	2.0	0.75	0.25	1.5
3	1.5	0.50	0.50	1.0
4	2.5	0.50	0.50	2.0
5	2.0	0.50	0.25	2.0
6	2.0	0.50	0.50	1.5
7	2.0	0.75	0.75	1.5
8	1.5	0.50	0.50	1.0
9	2.0	0.25	0.75	1.5
10	2.0	0.50	0.50	1.5
11	1.5	0.75	0.50	1.5
12	2.0	0.50	0.50	1.5
13	2.0	0.25	0.50	2.0
14	2.5	0.25	0.50	1.5
15	2.0	0.50	0.50	1.5
16	2.5	0.50	0.75	1.5
17	1.5	0.50	0.75	1.5
18	2.0	0.25	0.50	1.0
19	2.5	0.75	0.50	1.5
20	2.0	0.50	0.75	1.0
21	2.0	0.50	0.75	2.0
22	2.0	0.75	0.50	1.0
23	2.5	0.50	0.25	1.5
24	2.0	0.50	0.25	1.0
25	1.5	0.25	0.50	1.5
26	2.5	0.50	0.50	1.0
27	2.0	0.25	0.25	1.5
28	1.5	0.50	0.25	1.5
29	2.0	0.75	0.50	2.0
30	2.0	0.75	0.50	2.0

quantity (0.75 g) of CPT was also dispersed in this solution. Light liquid paraffin (120 mL) containing 1% v/v Span 80 and 0.1% v/v dimethyl polysiloxane was then placed in a 400-mL beaker and agitated with a three-blade propeller of 50-mm diameter linked to a homogenizer fitted with a four-blade "butterfly" propeller having a diameter of 50-mm (Virtis Company, New York, USA) to produce a homogenous oily phase. The entire volume of the acetone solution was poured into the oily continuous phase, and the system was maintained at 25 °C to evaporate the acetone. Processing variables such as the amount of liquid

paraffin and volume of acetone solution were maintained constant for all batches produced. After 2 h, 10 mL of *n*-hexane, the nonsolvent, was added to harden the microspheres, and stirring was continued for a further 5 h. The hardened microcapsules were collected using a Büchner funnel and washed 2–3 times with 50 mL *n*-hexane to remove any residual liquid paraffin. The microspheres were then dried at room temperature for 24 h. All batches were prepared in triplicate, and the dried microspheres were stored in well-closed containers. All experiments in which the evaluation of microspheres was undertaken were performed after 24 h.

Scanning Electron Microscopy (SEM)

The shape and surface morphology of the microspheres were investigated using SEM (Tescan, VEGA LMU, Czech Republic). The microspheres were mounted onto a double-sized carbon stub that was placed on a sample disc carrier (3-mm height, 10-mm diameter) and were coated with gold under vacuum (0.25 Torr) with a sputter coater (Balzers Union Ltd, Balzers, Lichtenstein). The samples were imaged using a 20 kV electron beam.

Drug Release Studies

A VanKel Bio-Dis dissolution apparatus (VanKel Industries, New Jersey, USA) was used for dissolution testing of microspheres manufactured in these studies. A model VK 750D digitally controlled water circulator/heater (VanKel Industries, New Jersey, USA) was used to maintain the temperature of the dissolution media at 37 ± 0.5 °C. Drug-loaded microspheres were tested in 250 mL of phosphate buffers of different pH values. The dissolution test was conducted at an agitation rate of 20 dips per minute (dpm). Samples (2 mL) were withdrawn and replaced with 2 mL of fresh medium, then automatically filtered through a 0.45-µm Durapore membrane HVLP filters (Millipore Corporation, Ireland). Samples were collected at predetermined time intervals after 1, 2, 6, 8, 10, and 12 h and quantified using a validated HPLC method (20). A summary of the dissolution test conditions used is listed in Table 2.

Samples were collected manually from vessels during pauses in the testing, and the percent CPT released from the microspheres after 12 h was calculated.

Mathematical Modeling

GraphPad Prism Software Version 5.0 (GraphPad Prism Software, San Diego, CA, USA) was used to fit the dissolution data generated following testing of all formulations, CPT-001–CPT-030. This software is used to estimate the parameters of a nonlinear function that provides the closest fit between experimental observations and the nonlinear function. The best-fit solution was identified by evaluating the coefficient of determination (R^2) and the sum of squares of residuals (SSR) where the highest R^2 value and smallest SSR values indicate the best fit (21–25).

Table 2. Summary of General Dissolution Conditions for Reciprocating Cylinder Dissolution Test Methods

Parameter	USP Apparatus 3
Dissolution medium	Buffers (pH 1.6, 3.4, 4.6, 6.8)
Temperature	37.0 ± 0.5 °C
Initial volume	250 mL
Basket/dip speed	20 dpm
Screen size	405 µm top /177 µm bottom
Filter size	0.45 µm
Volume drawn	2 mL
Dissolution time	1 h in pH 1.6 1 h in pH 3.4 5 h in pH 4.6 5 h in pH 6.8

The mathematical equations (26–36) for the models used to describe the dissolution curves for CPT formulations are summarized in Table 3.

RESULTS AND DISCUSSION

The IR absorption spectra (Figure 2) reveal that all characteristic bands for CPT are present in all spectra confirming that CPT and the excipients used in the manufacture of microspheres are unlikely to exhibit any deleterious incompatibilities.

During the initial stages of the dissolution process, the microspheres sank in the dissolution medium and subsequently swelled, after which they started to float, suggesting that the original density of the microspheres before matrix swelling in the dissolution medium was >1. The extent to which the microspheres floated depended on the balance between mass and volume differences of the microparticulate dosage form.

To elucidate the hydrodynamic conditions of importance when using USP Apparatus 3, Khamanga and Walker (37) postulated a simplified model of the fluid flow behavior around tablets in the apparatus. Laminar and turbulent flow patterns of microspheres that float while agitated at 20 dpm are depicted in Figure 3.

The black closed circles represent microspheres in a free-flowing test solution, and the strain on the system can be calculated from their movement. The shear strain is localized in the stagnant zone around the microspheres. The shear stress is applied parallel or tangentially to the microspheres, and the dissolution medium then imparts stress on the microspheres.

A reciprocating rate of less than 20 dpm would result in a free-stream velocity (unimpeded and with constant fluid flow), V_0 , that is lower than that which would predominate at higher agitation rates. The free-stream velocity is represented in the figures by lines that indicate the path of fluid around a microsphere suspended in a dissolution medium as the inner vessel reciprocates in and out of the

Table 3. Mathematical Representation of the Models Used to Fit CPT Release from Microcapsules

Model	Equation	Reference
Zero-order	$Qt = Q_0 + K_0t$	(26, 27)
First-order	$\ln Q_t = \ln Q_0 - K_1t$	(28, 29)
Higuchi	$Qt = Q_0 + K_Ht^{1/2}$	(30, 31)
Makoid–Banakar	$Qt = KMB t^n e^{(-ct)}$	(32)
Kopcha	$Qt = At^{1/2} + Bt$	(33)
Korsmeyer–Peppas	$Qt = K_{KP} t^n$	(34–36)

dissolution fluid. At lower dpm, the flow around the microspheres is smoother and more regular, and as agitation increases, a pseudo-laminar pattern predominates. Reciprocation rates of 20 dpm and greater may generate turbulence, which in turn, causes chaotic flow, and complex hydrodynamic patterns may occur in the fluids within the dissolution vessel. The fluid currents that are generated are likely to affect the microsphere mass at varying velocities in all directions, because the microspheres are spherical and present different angles to the direction of fluid flow. At this increased agitation rate, the intensity of the turbulence in all directions will likely be more pronounced. The higher reciprocation rate induces elevated fluid flow velocities and is consequently likely to weaken the gel structure that forms around a microsphere immediately at the commencement of hydration. As the gel layer weakens, the network that holds the polymeric structure intact slowly degrades, resulting in a depletion of the layer that ideally acts as the primary retarding region of the technology. Therefore, the drug is released more rapidly at higher agitation rates, because the surface exposure of the dosage form to the dissolution medium at a specific time is increased.

The turbulent flow observed at this agitation rate is characterized by chaotic or stochastic property changes, which is a nondeterministic behavior. Theoretically, there is low momentum diffusion, high momentum convection, and a rapid variation of velocity in space and time. Furthermore, during agitation the turbulent flow may cause the formation of eddies, and as the dissolution medium swirls, the microspheres are randomly shifted in all directions. At times, they may impact the cylinder wall, which in turn will facilitate the release of drug from the dosage form. In a transition flow state there is a mixture of both laminar and turbulent flow, with turbulence in the center of the cylinder and laminar flow occurring near the edges of the tube. In general, turbulent flow is characterized by left-to-right, right-to-left, up-and-down, and down-and-up movements but is highly disorganized. The microspheres move at high velocities, and the vector movements are completely irregular. In the inner cylinder where the dissolution medium also moves, a shearing stress is created at the cylinder wall, thereby retarding

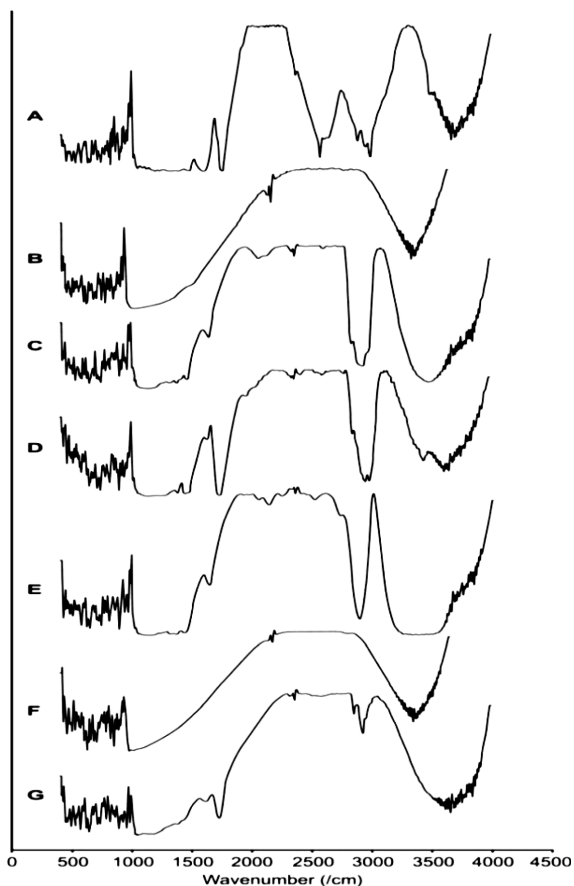


Figure 2. Infrared spectra of (A) CPT, (B) solid mixture of CPT with K15M, (C) K100M, (D) MCC, (E) Eudragit RS, (F) citric acid, and (G) all mixtures.

flow. This complex fluid movement, coupled with the effects of agitation rate, particle impact, and cylinder wall interactions, is postulated as the process that facilitates drug release from these microspheres.

The use of top screens of 177- μm mesh size resulted in poor dissolution medium drainage from the inner cylinders. The use of larger mesh screen/pore sizes allows air to penetrate through the mesh openings without difficulty and subsequently displace liquids that may be retained in the inner tubes. The use of a 405- μm mesh as the top screen resulted in better, more complete and rapid drainage of all cylinders, and the fluid flowed at a higher free-stream velocity, facilitating air penetration through the openings and subsequently displacing liquids that were retained in the inner tubes.

In the majority of cases, the microsphere formulations exhibited a burst release after which CPT was released at a constant rate. The burst effect of the drug is likely due to the turbulent effect of the dissolution medium in the reciprocating cylinder, which resulted in greater wetting and hydration of the microspheres. Ubrich et al. (38) reported that water-soluble drugs formulated in nanoparticles exhibit a tendency to migrate to the aqueous medium, thereby concentrating at the surface of

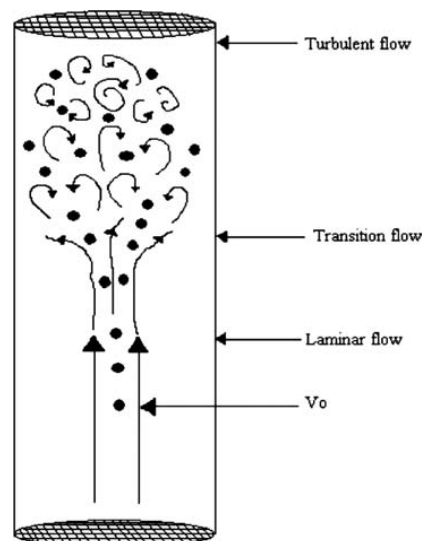


Figure 3. Laminar and turbulent flow patterns of microspheres agitated at 20 dpm in USP Apparatus 3.

particles, and involve the burst effect. These results are similar to those reported by Khamanga and Walker (37) when using USP Apparatus 3. Despite the spreading of the microspheres on the surface of the mesh, they are retained in the cylinder as they swelled following hydration.

The burst effect may also be attributed to the fact that some of the CPT microspheres had thin polymeric surfaces. The thin polymeric barrier together with the turbulent effect of the dissolution medium facilitates the entry of the dissolution medium into the microspheres, and therefore CPT leaches from the polymeric matrices of the microspheres exhibiting burst release. The burst effect may also occur if CPT is trapped on the surface of the polymeric matrix during the microencapsulation process and is therefore released as soon as the microspheres are placed in the dissolution medium. The migration of drugs during drying and storage of the microspheres may result in heterogeneous distribution of CPT in the polymeric matrix leading to burst release.

Instances of slow drug release could be attributed to the thick polymeric membrane surfaces of the microspheres, which formed an effective barrier and hindered the entry of the dissolution medium into the microsphere. The swelling nature of Methocel (HPMC) contributes to the buoyancy of the microspheres, and the addition of Eudragit RS decreased the permeability of the microspheres to the dissolution medium.

Eudragit RS has a low proportion of quaternary ammonium groups, which renders it less permeable to aqueous fluids. The use of this material decreased the porosity of the microsphere membrane to CPT, which may have resulted in a possible lag in the release of CPT from the microspheres. However, this was not observed since some CPT particles were trapped on the surface of the

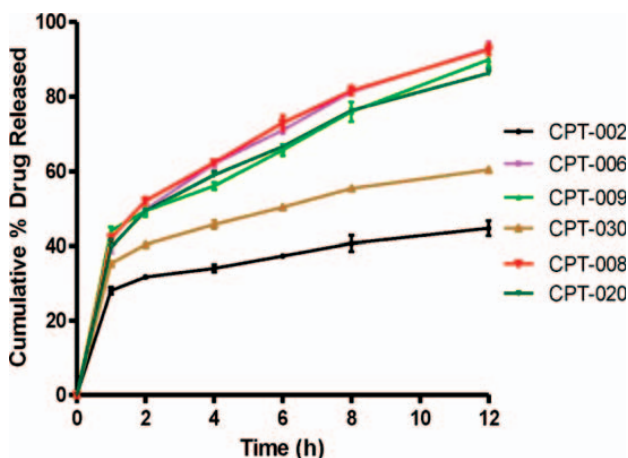


Figure 4. Cumulative percent drug released for batches CPT-002, 006, 008, 009, 020, and 030 (mean \pm SD, $n = 3$).

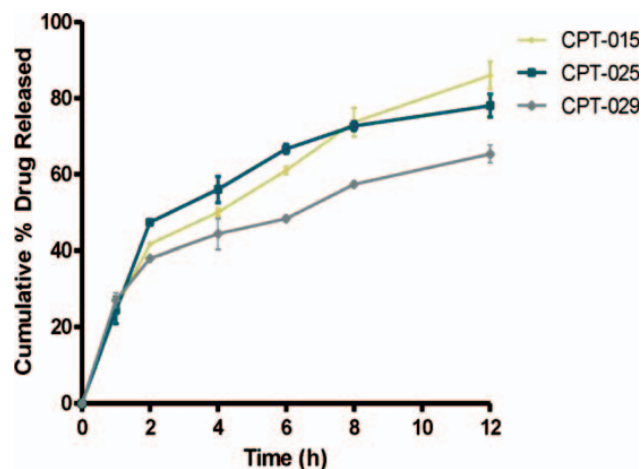


Figure 5. Cumulative percent drug released for batches CPT-015, 025, and 029 (mean \pm SD, $n = 3$).

polymer matrix. Furthermore, continual agitation by the reciprocating cylinder disrupted the polymer barrier, and this resulted in pore formation on the polymeric membrane surface, which further facilitated the penetration of the dissolution medium and enhanced CPT release. In all cases, approximately 70–90% CPT was released within 8–12 h. There is a paucity of information relating to the characterization and elucidation of the release mechanisms of CPT from floating microspheres.

The observations made in this study reveal that a combination of HPMC and Eudragit RS induces good floating ability to microspheres, and that control of drug release for an extended period of time is also possible. The microspheres that were produced had utmost floating tendency and exhibited satisfactory drug release.

Characteristic CPT release profiles from selected microsphere formulations are shown in Figures 4 and 5. The release profiles were constructed by plotting the percent drug released versus time. The decreased CPT release observed for some batches can be attributed to the development of a diffusional barrier between the CPT within the microspheres and the dissolution medium. The results show that the release rate of CPT from the microspheres could be modulated by adjusting the ratio of polymer/drug in the formulation and the speed of homogenization during manufacture.

During the formation of the microspheres, the presence of a low-viscosity dispersed phase delays polymer precipitation and solidification of the dispersed droplets. Consequently, additional water can diffuse into the droplets before solidification, forming pockets of water and pores in the walls of the microspheres. The more porous the particle wall, the easier it is for the dissolution medium to penetrate the particle; consequently, the dissolution of CPT from the microspheres is rapid. This phenomenon has also been reported by Pygall et al. (39). Moreover, the size of the microspheres decreases

significantly with a decreasing polymer/drug ratio; this also contributes to faster release of CPT when low polymer concentrations are used and may be a surface-area effect.

Typical SEM micrographs of selected microspheres are shown in Figure 6A–I. It is evident that the microspheres are not similar in shape, but most of the microspheres are discrete, spherical and uniform in shape and some have porous surfaces. At higher magnification, the microspheres have rough surfaces that are likely due to the presence of CPT, suggesting that the drug had not been efficiently encapsulated by the polymeric matrix. This may be due in part to the fact that the drug is thoroughly wetted, finely dispersed, and enveloped within the polymer matrix before encapsulation. In addition, the data from drug loading estimation confirmed that this was the case as the amount of CPT in these microspheres was greater than in others with smoother surfaces. However, this was not the case for batches CPT-006 and CPT-025 (Figure 6A,F) where CPT “particles” could be seen on the surfaces of the microspheres. The small microspheres produced in batch CPT-022 are shown in Figure 6I. Clearly, the small microspheres adhere to one another and form “grape-like” clusters. These microspheres were neither visually appealing nor free flowing and discrete as those of other batches.

The microspheres that were produced ranged in diameter between 30 and 200 μm , and the mean diameter was directly influenced by the manufacturing parameters (homogenizing speed and polymer concentration). Furthermore, larger particles were obtained at higher polymer/drug ratios. Increasing the polymer loading produced a more viscous solution, and when this solution was poured into the aqueous phase, larger droplets and thus larger microspheres were formed.

This burst-release phenomenon of CPT is evident in the dissolution profiles shown in Figure 4. Figure 5 shows experimentally fitted data and depicts drug release from

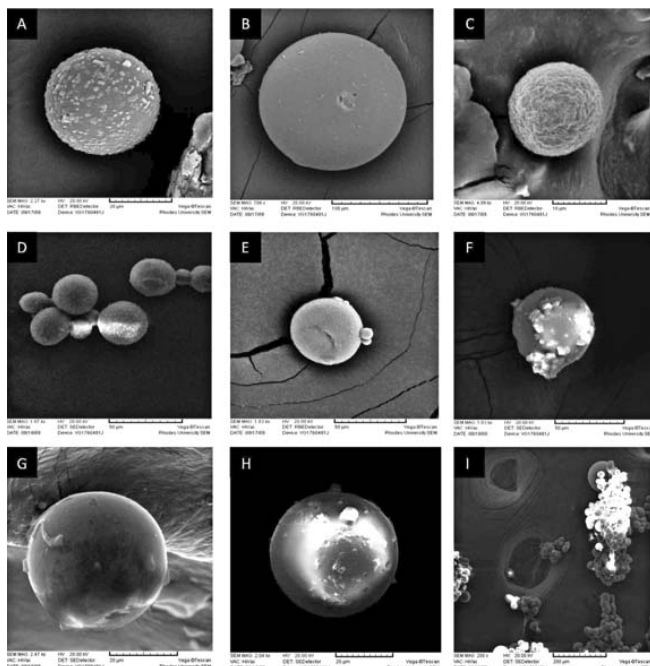


Figure 6. SEMs of CPT-loaded microspheres: (A) batch CPT-006, (B) batch CPT-002, (C) batch CPT-009, (D) batch CPT-020, (E) batch CPT-015, (F) batch CPT-025, (G) batch CPT-030, (H) batch CPT-029, and (I) batch CPT-022.

microspheres in which the burst release was minimal. The release profiles can be explained by the heterogeneous distribution of the drug within the matrix, as observed by SEM in some of the batches (Figure 6A,F). The profiles indicate that burst release was dominant in these batches of microspheres.

The low polymer levels used in these formulations resulted in more drug remaining at the surface of the microspheres, facilitating the initial and rapid release. The higher release rates are also associated with smaller and narrower size fractions of particles. SEM micrographs reveal drug crystals at or near the surfaces of the microspheres that dissolve quickly, and probably account for the observed rapid initial release. Almost all microsphere batches produced in this study revealed similar behavior.

During testing, a point is reached when the dissolution of solid drug particles results in the formation of continuous pores or channels within the matrix. Under these circumstances, drug release will follow the path of least resistance, and drug will diffuse through the channels to the bulk dissolution medium. Therefore, as the drug leaches out from the polymer, the matrix becomes more porous and faster drug release rates are observed.

The initial burst effect from HPMC matrices is a common occurrence when evaluating the release of water-soluble drugs (39, 40). Where drug release is retarded, it may be partly due to solid bridges that are formed between drug–drug and drug–excipient particles during processing. In addition, the internal pressure generated

from swelling and relaxation of the polymeric matrix may cause microrupturing of the particles during dissolution.

Most of the drug profiles appear to show two stages of dissolution. Initially, a burst effect corresponds to the rapid dissolution and release of CPT from the surfaces of the microspheres before formation of a gel membrane at the surface. Secondly, the release rate decreases continuously until the end of the process, possibly due to an increase in the diffusion path length for CPT, which is typical of a diffusion-controlled drug-release mechanism. Following the formation of a gel, drug release is controlled by drug diffusion across the gel layer. The burst effect is also dependent on the amount of drug present at the surface of the microspheres and the size and the shape of the pores generated within the microsphere structure during dissolution testing.

A further reason for a burst effect may be the unstable nature of inner emulsion droplets during solvent evaporation, which leads to coalescence and may have forced drug particles to migrate to the surface of the microspheres.

Despite the cracks that could be clearly observed in some microspheres, no bursting or collapsing of the microspheres was detected at the later stages of testing. The hypothesis is that following crack formation and exposure of new surfaces to the dissolution medium, tight and cohesive gel layers formed rapidly and were able to maintain and control drug release. In this way, the gel layer was able to “heal” or plug the crack, thereby protecting the integrity of the internal drug reservoir.

Mathematical Modeling

The curvilinear nature of the cumulative percent drug released versus time plots suggests that drug release from the microspheres does not follow zero-order kinetics. The data modeling results are summarized in Table 4, and this observation is supported by the low values of correlation coefficients obtained in all cases where the dissolution data were fitted to a zero-order model. The *in vitro* dissolution studies confirmed that drug release was governed by Higuchi kinetics, and the experimental data also adequately fit the Kopcha matrix model. However, the mathematical expression that best describes drug release from these microspheres is the Makoid–Banakar model in which the resultant R^2 values were greater than 0.98. The Korsmeyer–Peppas release exponent, n , is approximately 0.3, confirming that diffusion is the controlling factor for drug release. This finding is supported by evaluation of the ratios of the exponents A/B (i.e., diffusional term A and erosional term B) derived from the Kopcha model (33), which were greater than 1 in all cases. The Kopcha model can also be used to quantify the relative contributions of diffusion and polymer relaxation to drug release. The data in Table 4 clearly show that the value of A is far greater than that for B , suggesting that drug release from the microspheres is primarily controlled by a Fickian diffusion process.

Table 4. Results of Model Fitting of CPT Release Profiles

MODEL	FORMULATION																														
	CPT-001	CPT-002	CPT-003	CPT-004	CPT-005	CPT-006	CPT-007	CPT-008	CPT-009	CPT-010	CPT-011	CPT-012	CPT-013	CPT-014	CPT-015	CPT-016	CPT-017	CPT-018	CPT-019	CPT-020	CPT-021	CPT-022	CPT-023	CPT-024	CPT-025	CPT-026	CPT-027	CPT-028	CPT-029	CPT-030	
Zero-order																															
R^2	0.179	0.254	0.174	0.221	0.274	0.465	0.023	0.389	0.533	0.380	0.327	0.096	0.166	0.423	0.086	0.637	0.404	0.595	0.369	0.301	0.058	0.428	0.292	0.215	0.316	0.383	0.1856	0.239	0.319	0.303	
k_0	7.047	4.606	5.683	7.843	9.560	9.733	5.976	9.806	9.404	9.240	10.26	6.801	6.429	9.338	6.803	8.570	10.88	9.072	9.909	9.092	5.513	8.585	10.14	9.850	8.449	7.576	4.994	6.570	6.669	6.765	
SSR	6844	4198	6027	8801	11422	9190	5968	10387	7640	9238	12382	6852	5750	8934	7029	5199	13102	6423	10858	9896	4722	7465	12519	12955	8744	9094	4003	5555	7234	5474	
First-order																															
R^2	0.612	0.486	0.507	0.612	0.636	0.695	0.540	0.672	0.723	0.692	0.647	0.595	0.610	0.693	0.571	0.754	0.632	0.733	0.667	0.660	0.566	0.705	0.647	0.613	0.617	0.558	0.564	0.634	0.557	0.658	
k_1	28.10	20.63	24.99	29.94	37.03	35.18	25.40	36.53	32.92	34.10	39.14	27.71	25.72	34.17	28.08	28.46	40.85	30.80	37.19	34.68	22.91	31.15	38.97	39.03	32.64	31.68	20.83	25.69	28.09	25.83	
SSR	3238	1720	2526	4389	5718	5226	2678	5562	4531	4583	6479	3065	2685	4759	3295	3526	8086	4232	5728	4805	2177	3849	6240	6393	4901	4178	1776	2669	3195	2686	
Higuchi																															
R^2	0.852	0.673	0.717	0.767	0.895	0.954	0.934	0.968	0.914	0.915	0.829	0.855	0.934	0.829	0.985	0.934	0.977	0.929	0.891	0.818	0.935	0.903	0.881	0.910	0.815	0.796	0.881	0.794	0.897		
k_{Hi}	21.34	14.20	17.48	23.59	28.86	29.08	18.29	29.42	27.97	27.68	30.89	20.68	19.49	27.93	20.72	25.30	32.69	26.87	29.76	27.35	16.81	25.67	30.58	29.84	0.758	0.937	0.647	0.661	0.864	0.636	
SSR	1232	1093	1448	2626	1638	778.7	1249	1122	515.5	1280	1561	1296	996.8	1011	1309	208.2	1437	362.2	1224	1532	909.2	839.2	1703	1953	1140	1741	830.0	865.5	1479	802.2	
Makoid-Banakar																															
R^2	0.983	0.991	0.996	0.998	0.993	0.997	0.996	0.982	0.995	0.994	0.992	0.989	0.992	0.995	0.995	0.995	0.992	0.998	0.984	0.993	0.990	0.990	0.997	0.998	0.993	0.997	0.990	0.993	0.997	0.989	
k_{MB}	33.43	26.56	31.62	36.57	42.88	38.54	31.08	40.98	35.44	39.08	44.54	33.67	30.72	38.33	33.61	29.30	41.35	32.15	41.99	40.55	27.62	35.03	45.10	45.39	35.04	38.05	25.58	30.15	34.45	29.96	
n	0.263	0.165	0.184	0.266	0.291	0.352	0.219	0.326	0.376	0.317	0.308	0.241	0.260	0.334	0.244	0.424	0.521	0.406	0.319	0.292	0.237	0.336	0.295	0.287	0.432	0.251	0.225	0.279	0.221	0.296	
c	<0.001	<0.001	<0.001	<0.001	<0.001	<0.001	<0.001	<0.001	<0.001	<0.001	<0.001	<0.001	<0.001	<0.001	<0.001	<0.001	<0.001	<0.001	<0.001	<0.001	<0.001	<0.001	<0.001	<0.001	<0.001	<0.001	<0.001	<0.001	<0.001	<0.001	
SSR	136.4	28.47	19.91	1410	93.39	33.48	39.88	41.28	51.90	256.7	81.90	41.11	50.78	159.9	55.55	69.42	108.5	117.6	32.00	226.9	33.65	119.1	51.63	28.21	83.42	21.41	38.63	48.70	17.58	85.54	
Kopcha																															
R^2	0.852	0.673	0.717	0.767	0.895	0.954	0.934	0.968	0.914	0.915	0.829	0.855	0.934	0.829	0.985	0.931	0.977	0.929	0.891	0.818	0.935	0.903	0.881	0.910	0.815	0.796	0.881	0.794	0.897		
A	21.34	14.20	17.48	23.59	28.86	29.16	18.29	29.42	27.97	27.68	30.89	20.68	19.49	27.93	20.72	25.30	33.48	26.87	29.84	27.35	16.81	25.67	30.70	29.98	25.61	23.13	15.24	19.85	20.38	20.36	
B	<0.001	<0.001	<0.001	<0.001	<0.001	<0.001	<0.001	<0.001	<0.001	<0.001	<0.001	<0.001	<0.001	<0.001	<0.001	<0.001	<0.001	<0.001	<0.001	<0.001	<0.001	<0.001	<0.001	<0.001	<0.001	<0.001	<0.001	<0.001	<0.001	<0.001	
SSR	1232	1093	1448	2626	1638	779.3	1249	1122	515.5	1280	1561	1296	996.8	1011	1309	208.2	1498	362.2	1224	1532	909.2	839.2	1705	1955	1142	1741	830.0	865.5	1479	802.2	
Korsmeyer-Peppas																															
R^2	0.980	0.991	0.996	0.955	0.991	0.998	0.993	0.999	0.998	0.994	0.996	0.994	0.992	0.992	0.995	0.998	0.989	0.998	0.989	0.998	0.993	0.997	0.998	0.998	0.998	0.990	0.992	0.998	0.993	0.989	
k_{KP}	33.85	26.61	31.66	44.49	43.94	39.45	31.07	42.33	37.06	42.83	45.27	33.75	30.72	40.59	33.60	30.54	41.37	33.29	43.37	43.45	27.63	37.57	45.14	34.89	38.00	25.62	30.22	34.50	30.07		
n	0.252	0.165	0.184	0.0173	0.263	0.327	0.219	0.281	0.325	0.222	0.275	0.241	0.260	0.269	0.244	0.380	0.398	0.368	0.272	0.213	0.237	0.270	0.291	0.294	0.353	0.240	0.225	0.278	0.221	0.295	
SSR	130.6	28.45	19.90	228.7	60.25	9.489	39.88	6.021	8.193	44.95	28.06	41.05	50.78	58.96	55.55	32.92	13.93	78.02	8.300	85.20	33.65	15.36	11.51	12.01	57.16	15.06	38.62	48.62	17.57	85.39	

The results of curve-fitting studies reveal that CPT release from the microspheres could be best described by the Makoid–Banakar, Korsmeyer–Peppas, Kopcha, and Higuchi models. The R^2 values were >0.900 for all analyses, and the corresponding sum-of-squared residual (SSR) values were lower than those of the other models. The formulations with low levels of rate-controlling polymers exhibited a higher burst release, which can be ascribed to the dissolution of the CPT from the surface of the microspheres. Furthermore, the balance that exists between the swelling and gelling characteristics of the microspheres is vital to ensure and maintain the desired release rates for CPT.

It is most important to consider the suitability, predictive ability, and accuracy of any model chosen to describe the release process when developing new pharmaceutical products or evaluating drug release mechanisms. The presence of a highly water-soluble drug in an HPMC matrix can generate an osmotic gradient. This may result in a greater rate of polymer swelling and an increase in gel thickness with a corresponding initial increase followed by a drastic decrease in the rate of drug release (41).

It should be noted that the value of R^2 alone is not an exact measure of the accuracy of a model but is a measure of the reduction in the variability of a response generated by use of additional variables in a model. However, a large value for R^2 does not necessarily imply that the regression model used is a good model. As is shown in Table 4, the addition of another variable to a model increased the value of R^2 irrespective of the statistical significance the additional variable.

CONCLUSION

The release mechanisms of microspheres manufactured using Eudragit RS, Methocel K100M, and Methocel K15M were assessed and were affected by the degree of polymer swelling. The selection of an appropriate model for the analysis of drug release provided insight into the underlying mass transport mechanism of release from the delivery technologies. The value of the release exponent, n , was <0.45 indicating that CPT release was controlled not only by diffusion. Fitting of data to the Kopcha model supported the evidence that CPT release involved a combination of a diffusion-controlled and a chain relaxation–swelling mechanism for most formulations.

Considerable attention must be focused on understanding the mathematical models used to describe pharmaceutical processes, as these provide a useful guide and insight into drug release and transport mechanisms from sustained-release technologies.

The stress induced by the hydrodynamic effects of the dissolution medium result in shear stress and erosion of the microspheres, which result in high collision with the reciprocating cylinder. Visual inspection of the microspheres showed that swelling was a dominant process, and minute drug particles were still passed

through the mesh screen, suspended, and finally precipitated at the bottom of the vessels.

The present investigation of floating microspheres using polymer combinations of Eudragit RS and HPMC is ideal as it releases the drug in controlled fashion for extended periods by maintaining buoyancy. The high permeability of Eudragit RS gives the initial burst release, which is desirable from therapeutic point of view.

ACKNOWLEDGMENTS

The authors are grateful to the National Research Foundation (RBW), Joint Research Committee of Rhodes University (SMK, RBW), and the Andrew W. Mellon Foundation (SMK) for financial support.

REFERENCES

1. Gianotto, E. A.; Arantes, R. P.; Lara-Filho, M. J.; Filho, A. C. S. C.; Fregonezi-Nery, M. M. Dissolution test for glibenclamide tablets. *Quim. Nova* **2007**, *30* (5), 1218–1221.
2. Costa, P.; Sousa Lobo, J. M. Modeling and comparison of dissolution profiles. *Eur. J. Pharm. Sci.* **2001**, *13* (2), 123–133.
3. Hanson, R.; Gray, V. *Handbook of Dissolution Testing*, 3rd ed.; Dissolution Technologies, Inc.: Hockessin, DE, 2004.
4. Kanfer, I. Workshop Report-Challenges in Dissolution Testing: Equivalence and Surrogates. *Dissolution Technol.* **2010**, *17* (3), 41–50.
5. Underwood, T.; Cadwalladaer, D. Automated potentiometric procedure for studying dissolution kinetics of acidic drugs under sink conditions. *J. Pharm. Sci.* **1978**, *67* (8), 1163–1167.
6. Chiou, W. I.; Riegelman, S. Oral absorption of griseofulvin in dogs: increased absorption via solid dispersion in polyethylene glycol 6000. *J. Pharm. Sci.* **1970**, *59* (7), 937–941.
7. García, C. V.; Paim, C. S.; Steppe, M.; Schapoval, E. E. S. Development and validation of a dissolution test for rabeprazole sodium in coated tablets. *J. Pharm. Biomed. Anal.* **2006**, *41* (3), 833–837.
8. Reddy, K. R.; Mutalik, S.; Reddy S. Once-Daily Sustained-Release Matrix Tablets of Nicorandil: Formulation and In Vitro Evaluation. *AAPS PharmSciTech* **2003**, *4* (4), 480–488. <http://www.springerlink.com/content/7104416110g33lp7/fulltext.pdf> (accessed Jan 15, 2012).
9. Kim, H.; Fassihi, R. A new ternary polymeric matrix system for controlled drug delivery of highly soluble drugs. I. Diltiazem hydrochloride. *Pharm. Res.* **1997**, *14* (10), 1415–1421.
10. Williams, T. A.; Corvol, P.; Soubrier, F. Identification of Two Active Site Residues in Human Angiotensin I-converting Enzyme. *J. Biol. Chem.* **1994**, *269* (47), 29430–29434.
11. Williams, T. A.; Michaud, A.; Houard, X.; Chauvet, M.-T.; Soubrier, F.; Corvol, P. *Drosophila melanogaster* angiotensin I-converting enzyme expressed in *Pichia pastoris* resembles the C domain of the mammalian homologue and does not require glycosylation for

- secretion and enzymic activity. *Biochem. J.* **1996**, *318*, 125–131.
12. Ooi, H.; Colucci, W. Pharmacological Treatment of Heart Failure. In *Goodman and Gilman's The Pharmacological Basis of Therapeutics*, 10th ed.; Hardman, J. G., Limbird, L. E., Eds.; McGraw Hill: New York, 2001; p 910.
 13. Ondetti, M. A.; Cushman, R. B. D. W. Design of specific inhibitors of angiotensin-converting enzyme: New class of orally active antihypertensive agents. *Science* **1977**, *196* (4288), 441–444.
 14. Wilding, I. R.; Davis, S. S.; Bakhshae, M.; Stevens, H. N. E.; Sparrow, R. A.; Brennan, J. Gastrointestinal transit and systemic absorption of captopril from a pulsed-release formulation. *Pharm. Res.* **1992**, *9* (5), 654–657.
 15. Aboul-Enein, H. Y.; Al-Badr, A. A.; Ibrahim, S. E. Salbutamol. In *Analytical Profiles of Drug Substances*; Flory, K., Ed.; Academic Press, Inc.: New York, 1981; Vol. 10, p 665.
 16. Worland, P. J.; Drummer, O. H.; Jarrott, B. Gastric and intestinal absorption of captopril in acutely and chronically treated rats: Comparison with salicylic acid. *J. Pharm. Sci.* **1984**, *73* (12), 1755–1758.
 17. Macêdo, R. O.; Gomes do Nascimento, T.; Soares Aragão, C. F.; Barreto Gomes, A. P. Application of Thermal Analysis in the Characterization of Anti-hypertensive Drugs. *J. Therm. Anal. Calorim.* **2000**, *59* (3), 657–661.
 18. Sweetman, S. C., Ed. *Martindale, the Complete Drug Reference*, 35th ed.; Pharmaceutical Press: London, 2007; pp 1112–1113.
 19. Khamanga, S. M.; Parfitt, N.; Nyamuzhiwa, T.; Haidula, H.; Walker, R. B. The Evaluation of Eudragit Microcapsules Manufactured by Solvent Evaporation Using USP Apparatus 1. *Dissolution Technol.* **2009**, *16* (2), 15–22.
 20. Khamanga, S. M.; Walker, R. B. The use of experimental design in the development of an HPLC-ECD method for the analysis of captopril. *Talanta* **2011**, *183* (3), 1037–1049.
 21. Kumar, P.; Singh, S.; Mishra, B. Development and biopharmaceutical evaluation of extended release formulation of tramadol hydrochloride based on osmotic technology. *Acta Pharmaceut.* **2009**, *59* (1), 15–30.
 22. Sonnergaard, J. M. On the misinterpretation of the correlation coefficient in pharmaceutical sciences. *Int. J. Pharm.* **2006**, *321* (1–2), 12–17.
 23. Hunter, J. S. Calibration and the straight line: current statistical practices. *J. Assoc. Off. Anal. Chem.* **1981**, *64*, 574–583.
 24. Badino, A. C. Jr.; Facciotti, M. C. R.; Schmidell, W. Volumetric oxygen transfer coefficients ($k_L a$) in batch cultivations involving non-Newtonian broths. *Biochem. Eng. J.* **2001**, *8*, 111–119.
 25. Corbett, B. M. Selecting a best-fit temperature-dependent regression model for thin target HVI data. *Int. J. Impact Eng.* **2008**, *35* (12), 1672–1677.
 26. Donbrow, M.; Samuelov, Y. Zero order drug delivery from double-layered porous films: release rate profiles from ethyl cellulose, hydroxypropyl cellulose and polyethylene glycol mixtures. *J. Pharm. Pharmacol.* **1980**, *32* (7), 463–470.
 27. Varelas, C. G.; Dixon, D. G.; Steiner, C. A. Zero-order release from biphasic polymer hydrogels. *J. Control. Release.* **1995**, *34* (3), 185–192.
 28. Gibaldi, M.; Feldman, S. Establishment of sink conditions in dissolution rate determinations. Theoretical considerations and application to nondisintegrating dosage forms. *J. Pharm. Sci.* **1967**, *56* (10), 1238–1242.
 29. Wagner, J. G. Interpretation of percent dissolved time plots derived from in vitro testing of conventional tablets and capsules. *J. Pharm. Sci.* **1969**, *58* (10), 1253–1257.
 30. Higuchi, T. Rate of release of medicaments from ointment bases containing drugs in suspension. *J. Pharm. Sci.* **1961**, *50* (10), 874–875.
 31. Higuchi, T. Mechanism of sustained-action medication. Theoretical analysis of rate of release of solid drugs dispersed in solid matrices. *J. Pharm. Sci.* **1963**, *52* (12), 1145–1149.
 32. Pais, J. Intuiting Mathematical Objects Using Diagrams and Kinetigrams. *JOMA* **2001**, *1* (2). <http://mathdl.maa.org/mathDL/4/?pa=content&sa=viewDocument&nodid=429> (accessed Jan 12, 2012).
 33. Kopcha, M.; Lordi, N. G.; Tojo, K. J. Evaluation of release from selected thermosoftening vehicles. *J. Pharm. Pharmacol.* **1991**, *43* (3), 382–387.
 34. Korsmeyer, R. W.; Peppas, N. A. Macromolecular and modeling aspects of swelling-controlled systems. In *Controlled Release Delivery Systems*; Roseman, T. J., Mansdorf, S. Z., Eds.; Marcel Dekker, Inc.: New York, 1981.
 35. Korsmeyer, R. W.; Gurny, R.; Doelker, E. M.; Buri, P.; Peppas, N. A. Mechanism of solute release from porous hydrophilic polymers. *Int. J. Pharm.* **1983**, *15* (1), 25–35.
 36. Peppas, N. A. Analysis of Fickian and non-Fickian drug release from polymers. *Pharm. Acta. Helv.* **1985**, *60* (4), 110–111.
 37. Khamanga, S. M. M.; Walker, R. B. The Effects of Buffer Molarity, Agitation Rate, and Mesh Size on Verapamil Release from Modified-Release Mini-Tablets Using USP Apparatus 3. *Dissolution Technol.* **2007**, *14* (2), 19–23.
 38. Ubrich, N.; Bouillot, P.; Pellerin, C.; Hoffman, M.; Maincent, P. Preparation and characterization of propranolol hydrochloride nanoparticles: a comparative study. *J. Control. Release* **2004**, *97* (2), 291–300.
 39. Pygall, S. R.; Kujawinski, S.; Timmins, P.; Melia, C. D. Mechanisms of drug release in citrate buffered HPMC matrices. *Int. J. Pharm.* **2009**, *370* (1–2), 110–120.
 40. Bravo, S. A.; Lamas, M. C.; Salomon, C. J. Swellable matrices for the controlled-release of diclofenac sodium: Formulation and in vitro studies. *Pharm. Dev. Technol.* **2004**, *9* (1), 75–83.
 41. Ebube, N. K.; Jones, A. B. Sustained release of acetaminophen from a heterogeneous mixture of two hydrophilic non-ionic cellulose ether polymers. *Int. J. Pharm.* **2004**, *272* (1–2), 19–27.